Linked mechanical and biological aspects of remodeling in mouse pulmonary arteries with hypoxia-induced hypertension

Ryan W. Kobs, Nidal E. Muvarak, Jens C. Eickhoff and Naomi C. Chesler

AJP - Heart 288:1209-1217, 2005. First published Nov 4, 2004; doi:10.1152/ajpheart.01129.2003

Am J Physiol Heart Circ Physiol 288: H1209–H1217, 2005.
First published November 4, 2004; doi:10.1152/ajpheart.01129.2003.

Linked mechanical and biological aspects of remodeling in mouse pulmonary arteries with hypoxia-induced hypertension

Ryan W. Kobs,[1] Nidal E. Muvarak,[1] Jens C. Eickhoff,[2] and Naomi C. Chesler[1]

Departments of [1]Biomedical Engineering and [2]Biostatistics and Medical Informatics, University of Wisconsin, Madison, Wisconsin

Submitted 1 December 2003; accepted in final form 22 October 2004

Kobs, Ryan W., Nidal E. Muvarak, Jens C. Eickhoff, and Naomi C. Chesler. Linked mechanical and biological aspects of remodeling in mouse pulmonary arteries with hypoxia-induced hypertension. *Am J Physiol Heart Circ Physiol* 288: H1209–H1217, 2005. First published November 4, 2004; doi:10.1152/ajpheart.01129.2003.—Right heart failure due to pulmonary hypertension causes significant morbidity and mortality. To study the linked vascular mechanical and biological changes that are induced by pulmonary hypertension, we mechanically tested isolated left main pulmonary arteries from mice exposed to chronic hypobaric hypoxia and performed histological assays on contralateral vessels. In isolated vessel tests, hypoxic vessels stretched less in response to pressure than controls at all pressure levels. Given the short length and large diameter of the pulmonary artery, the tangent Young's modulus could not be measured; instead, an effective elastic modulus was calculated that increased significantly with hypoxia [(280 kPa (SD 53) and 296 kPa (SD 50) for 10 and 15 days, respectively, vs. 222 kPa (SD 35) for control; $P < 0.02$)]. Hypoxic vessels also had higher damping coefficients [(0.063 (SD 0.017) and 0.054 (SD 0.014) for 10 and 15 days, respectively, vs. 0.033 (SD 0.016) for control; $P < 0.002$)], indicating increased energy dissipation. The increased stiffness with hypoxia correlated with an increase in collagen thickness (percent collagen multiplied by wall thickness) as well as the sum of elastin and collagen thicknesses measured histologically in the artery wall. These results highlight the mechanobiological changes in the pulmonary vasculature that occur in response to hypoxia-induced pulmonary hypertension. Furthermore, they demonstrate significant vascular mechanical and biological changes that would increase pulmonary vascular impedance, leading to right heart failure.

pulmonary hypertension; elastic modulus; damping; elastin; collagen

PULMONARY HYPERTENSION is a potentially fatal disease, resulting from chronic obstructive or interstitial lung disease, recurrent pulmonary emboli, antecedent heart disease, hypoxia, or other unknown causes (5, 37). Experimentally, pulmonary hypertension is often generated with hypoxia, either by increasing the environmental nitrogen content or by decreasing ambient pressure to hypobaric conditions; in either case, the reduced oxygen availability causes pulmonary vasoconstriction and hypertension (10, 29, 40). The response to hypobaric hypoxia has been widely studied in calves (39, 43), pigs (12), rats (18, 27, 36), and wild-type and transgenic mice (10, 32, 35). In all of these animal models, as well as in humans (5), pulmonary hypertension leads to changes in pulmonary vascular structure (i.e., pulmonary vascular remodeling).

Pulmonary vascular remodeling in response to pulmonary hypertension is typically characterized by thickening in each of the three layers of the blood vessel wall by a combination of intimal and smooth muscle cell hypertrophy and hyperplasia and increased collagen, elastin, and fibronectin deposition (21). In response to hypoxia, the most dramatic structural vascular changes in rats are in the main (hilar) pulmonary arteries, which thicken through protein accumulation, and in the small arteries and arterioles, which thicken medially through muscularization (30). Various growth-related genes have been shown to modulate these structural changes in hypoxia-induced pulmonary hypertension, including transforming growth factor-β (34), platelet-derived growth factor (22), endothelin-1, and endothelin receptor (7, 9, 25, 33), as well as extracellular matrix-related genes such as the type I procollagen, tropoelastin, and fibronectin genes (8, 38). However, the mechanical changes resulting from these structural and gene-level changes are not well understood.

In situ, the elastic moduli of collagen and elastin have been measured to be 10 and 3.0 MPa, respectively, whereas the moduli of active and passive vascular smooth muscles cells have been estimated to be 2.0 and 0.1 MPa, respectively (17). The contribution of extracellular matrix proteins to whole tissue mechanics depends on their spatial distribution, orientations, and connections; similarly, the contribution of smooth muscle cells (SMCs) depends on their amount and level of contractile activity (20). In particular, Cox found that the amount of viscoelasticity in canine pulmonary arteries correlated with the amount of SMCs (6). Other investigators claim that proteoglycans and ground substances are important contributors to arterial viscous properties (26). Because the elastic moduli and viscoelasticity of pulmonary arteries affect the compliance of the pulmonary vasculature, which directly affects the pump work required of the right heart (31), understanding the changes in mechanical-functional behavior of the pulmonary vasculature with hypertension is critical to predicting and possibly preventing right heart failure. Therefore, the goal of this study was to quantify the mechanical properties of pulmonary arteries during pulmonary vascular remodeling and to correlate these mechanical changes with biological changes such as collagen and elastin accumulation.

Hypertension was generated in mice by lowering ambient conditions to one-half atmospheric pressure (380 mmHg) for 10 and 15 days. This degree of hypoxia has been shown to increase mouse pulmonary artery pressures nearly 50%, from 23 to 33 mmHg in C57BL/6 mice (32). In response to this stimulus, we hypothesized that wall thickening would occur primarily by adventitial collagen and intima-medial elastin

Address for reprint requests and other correspondence: N. C. Chesler, Dept. of Biomedical Engineering, Univ. of Wisconsin-Madison, Rm. 2146, Engineering Centers Bldg., 1550 Engineering Dr., Madison, WI 53706-1609 (E-mail: chesler@engr.wisc.edu).

The costs of publication of this article were defrayed in part by the payment of page charges. The article must therefore be hereby marked "*advertisement*" in accordance with 18 U.S.C. Section 1734 solely to indicate this fact.

accumulation, that static stretch would be reduced primarily by the increase in collagen (the stiffer of the two extracellular matrix proteins), that the dynamic tissue modulus (E) would increase because of the increase in collagen (again, the stiffer protein), and that the damping coefficient would increase with a increase in SMC thickness. We tested these hypotheses with isolated vessel experiments on the left main pulmonary arteries and quantitative histology on the right main pulmonary arteries of mice exposed to 0 (control), 10, and 15 days of hypobaric hypoxia.

METHODS

Animal handling. Twenty-seven 6-wk-old C57BL/6J male mice (Jackson Laboratory, Bar Harbor, ME) were randomly divided into three groups: 0-day control, 10-day hypoxic, and 15-day hypoxic (n = 9 each). The latter two groups were exposed to hypoxia in the University of Wisconsin Biotron facility; an equivalent inspired O_2 level of 10% was created with a barometric pressure of 380 mmHg (equivalent to an altitude of ~16,800 ft). Ambient pressure returned to atmospheric conditions (760 mmHg) for no more than 30 min once per day for regular animal care and maintenance. Mice were euthanized with an intraperitoneal injection of 5.0 μl/g pentobarbital solution. We report data from eight control animals because one experiment failed before data collection. All protocols and procedures were approved by the University of Wisconsin Institutional Animal Care and Use Committee.

Experimental manipulation. Upon excision of the heart and lungs, the left and right pulmonary arteries (PAs) were cleared of excess connective tissue, excised between the first and second PA bifurcations, and placed in fresh Dulbecco's phosphate-buffered saline solution (PBS; without calcium chloride or magnesium chloride; Sigma Chemical, St. Louis, MO). The left PA was mounted in an arteriograph system for mechanical testing, while the right PA was preserved for histology in frozen sections. Preliminary experiments demonstrated some minor histological changes after mechanical testing (such as wall thinning by adventitial compaction), so left and right arteries were used for the mechanical and biological assays, respectively.

Mechanical testing. The arteriograph chamber (Living Systems Instrumentation, LSI; Burlington, VT) consisted of a bath for superfusion and a set of proximal and distal glass microcannulas (tip = 400 μm) on which the artery was mounted and secured with single strands of nylon suture (diameter = 10 μm). The base of the chamber was a thin glass coverslip through which the vessel was visualized by transillumination microscopy. An attached video camera and video dimension analyzer (LSI) allowed viewing and electronic measurement of vessel dimensions. In particular, lumen diameter and left and right wall thicknesses were quantified (±1.0 μm) by the video scan line as described previously (3).

Thus mounted, vessels were perfused with PBS through the proximal microcannula driven by a multi-roller pump. PBS was used to fill the arteriograph bath, buffered to maintain a constant pH of 7.4, and heated to 37°C. Pressure transducers were situated immediately up- and downstream of the vessel. An upstream in-line pressure servomechanism (LSI) continually adjusted the computed average transmural pressure via computer control (LabVIEW; National Instruments, Austin, TX). The distal microcannula was then closed off to flow, and a transmural pressure was applied to the vessels.

Immediately after mounting, the left PA was pressurized to 5 mmHg, and its length was measured from suture to suture. The average suture-to-suture length was 2.2 mm (SD 0.3). The vessel was then stretched on average 112% (SD 2), which was sufficient to prevent buckling at higher pressures. We could not mimic in vivo axial strain (150% in rat PAs; Ref. 19) without catastrophic failure of the experiment by the vessel pulling off the microcannulas. However, because all vessels were stretched the same amount relative to their length, differences between control and hypoxic groups should hold.

Next, the vessel was mechanically preconditioned by cycling the pressure five times from 5 to 25 mmHg at 0.014 Hz. The response was repeatable after the third cycle in general. The fifth cycle of data was used to calculate the dynamic circumferential modulus and damping coefficient. For static properties, the vessel was subjected to five pressure steps; these were from 5 to 10, 5 to 15, 5 to 20, 5 to 25, and finally 5 to 10 mmHg for 45 s each. Steps were separated by 10 times the step duration (450 s) of rest at 5 mmHg to allow tissue recovery from previous steps (23). Upstream and downstream pressure, inner diameter, and left and right wall thicknesses were sampled at 1 Hz and saved on a PC for further analysis.

All experiments were performed after appropriate mechanical preconditioning in calcium-free medium to eliminate time- and pressure-dependent changes in SMC activity. That is, the passive but not active mechanical properties of the PAs were measured. Because we were not explicitly interested in the contractile state of the SMCs, endothelial and SMC viability was not tested with vasoactive agents as has been described previously (11). However, both of these cells types were found to be present and intact in vessels after mechanical testing histologically (data not shown).

Calculations. For the purposes of the mechanical analysis, the artery wall is assumed to be incompressible and homogeneous. With the thin wall assumption, which is valid for radius-to-wall thickness (WT) ratio >10, circumferential wall stress (σ) was calculated according to

$$\sigma = \frac{\mathrm{ID}}{2\mathrm{WT}}\mathrm{P} \qquad (1)$$

where P is the transmural pressure and ID is the inner diameter. Circumferential strain (e) was calculated with the use of Almansi's formulation for large deformations (14), based on circumferential stretch (λ), which is the ratio of pressure-dependent, deformed circumference [$\pi \cdot$outer diameter (OD)] to circumference at the baseline pressure of 5 mmHg ($\pi \cdot \mathrm{OD}_5$)

$$e = \frac{1}{2}\left(1 - \frac{1}{\lambda^2}\right) \text{ where } \lambda = \frac{\pi \mathrm{OD}}{\pi \mathrm{OD}_5} = \frac{\mathrm{OD}}{\mathrm{OD}_5} \qquad (2)$$

Unlike thick walled arteries, PAs are prone to collapse at zero transmural pressure; thus a non-zero baseline pressure is typically used (11). Collapse is to be avoided, since it is likely to damage endothelial cells. Thus the vessel state at 5 mmHg was used as an approximation of the unloaded state, which was used as the reference state in all calculations. The zero-stress state, which can be assessed with opening angle experiments, is often used as the reference state to account for residual stresses in thick walled vessels (14). In general, residual stresses in blood vessels act to equalize the radial distribution of circumferential stresses in the pressurized state (13). In thin walled vessels, a mean circumferential stress is computed, and the effects of residual stresses can be ignored.

The static stretch response of the vessel was analyzed isochronally, 15 s into the pressure step. Given the short length and large diameter of the PA in vivo and in the isolated vessel configuration, ideal test conditions for measuring tissue elasticity were not attainable even in principle. Therefore, we defined an effective dynamic circumferential elastic modulus E based on this partially constrained tissue geometry. E was calculated as the slope of the stress-strain curve near the midstrain point ($e_{50\%}$) during dynamic loading (see Fig. 1; note that e is dimensionless, as indicated by a dash in place of units in the x-axis label). In particular, the slope of the line best fit to the 10 data points nearest to the midstrain point was used. This effective elastic modulus likely differs in a consistent way from the tangent Young's modulus of the tissue due to end effects, since the aspect ratio was relatively consistent for the specimens (~3–3.5), as determined by their anatomy.

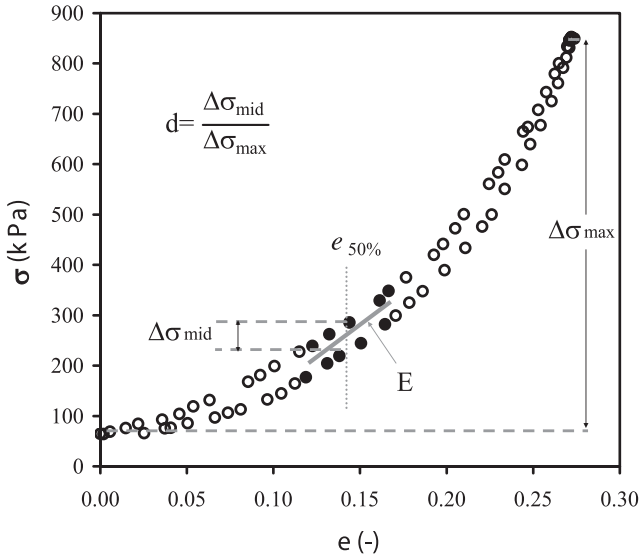

Fig. 1. Representative pulmonary artery (PA) dynamic stress-strain curve (10-day vessel). Stress σ is computed from *Eq. 1*; strain e is computed from *Eq. 2* (see *Calculations*). Open circles represent values obtained during inflation and deflation. Closed circles represent the 10 data points closest to the midstrain point ($e_{50\%}$), from which effective elastic modulus *E* was computed. Damping coefficient was computed as shown (and described in the text).

The damping coefficient was also calculated from dynamic-loading stress-strain relationship (23); the stress difference between inflation and deflation at the midstrain point, divided by the stress difference between the maximum and minimum stress values over the whole cycle, was used (Fig. 1).

Note, WT was optically measured under the conditions where accuracy and precision were the highest (25 mmHg), and then conservation of mass (assuming no axial extension) was used to find the WT value at any pressure. That is, for all of the above calculations, the pressure-dependent WT was calculated as in Ref. 11, using the formula

$$WT = \frac{OD - \sqrt{OD^2 - OD_{25}^2 + ID_{25}^2}}{2} \quad (3)$$

where OD is the pressure-dependent outer diameter as defined above, and ID_{25} and OD_{25} are the inner and outer diameters, respectively, measured at a transmural pressure of 25 mmHg. This method, which has been validated by Faury et al. (11) in isolated vessels experiments, was used because the optically measured WT values were not reliable at low pressures due to poor contrast at the vessel wall-to-fluid interfaces, a consequence of the greater circumferential wall curvature.

Histology. The right main PA was slow frozen in tissue-freezing medium surrounded by 2-methyl butane cooled by liquid nitrogen. Vessels were frozen at nearly zero transmural pressure without chemical fixing to enable future measurement of enzymatic activity with an assay such as in situ zymography (4). At least two 5-μm sections were cut at −20°C on a cryostat from the proximal and distal ends of each vessel for each assay. These sections were stained with Verhoff Van Geisen (VVG) solution to identify elastin (1), picro-sirius red (SR) to identify collagen (16), and hematoxylin to measure intimal to adventitial *WT*. Sections were imaged on an inverted microscope (TE-2000; Nikon, Melville, NY) and captured using a Spot camera and software for image capture and analysis (MetaVue; Optical Analysis Systems, Nashua, NH). For the VVG and SR stains, two representative fields of view (FOV) were chosen for each location (proximal or distal) by a single observer blinded to the experimental condition. The area positive for protein (elastin or collagen) was identified by color thresholding in the FOV (black for elastin by VVG, red for collagen by SR) and compared with the total tissue area in the FOV to produce a percent protein in the artery wall. SMC percentage was computed with the assumption that endothelial cells, ground substances, and other components contributed minimally to the vessel thickness. That is, SMC% = 100% − (elastin%) − (collagen%) for each vessel.

WT was measured with line measurement tools (after appropriate calibration) by averaging 10–12 equally spaced positions around the whole vessel circumference for each location (proximal or distal). These measurements were also taken by a single individual blinded to the experimental condition.

For collagen, elastin, and SMC percentages and WT, no significant differences were found between the proximal and distal locations. Therefore, data for each vessel were pooled to generate a length-wise average value for each measurement. Also, collagen (or elastin or SMC) thickness was computed as the percent collagen (or elastin or SMC) multiplied by the average WT for each vessel.

Statistics. On the basis of our previous work with mouse PAs (3), we anticipated that the difference in mean vessel elastic modulus between the experimental and control groups would be at least 1.5 standard deviations (SD; or an effect size of 1.5). A sample size of nine animals per group (27 in total) was chosen to detect a difference of 1.5 SD in mean vessel elastic modulus difference between two study arms with 85% power at a two-sided significance level of 0.05. These calculations use the standard Student's *t*-test with equal SD for the significance test, assuming normality in the data. As noted above, we report data from eight control experiments because one experiment failed before data collection.

ANOVA models were used to examine differences in vessel dynamic behavior, collagen thickness, elastin thickness, SMC thickness, and *WT* between the experimental groups (0-, 10-, and 15-day). Repeated-measurement ANOVA models were used to examine differences in vessel static behavior, collagen percentage, elastin percentage, and SMC percentage between the experimental groups. All results are presented as mean ± SD. Analyses of correlation between the mechanical-functional and histological-biological measurements were performed using nonparametric Spearman's rank correlation coefficient. The regression analysis coefficient of determination (R^2) is reported to reflect the linearity of the correlative relationships; Spearman's correlation coefficient (r_s) and its associated *P* value (if significant) are reported to reflect the trends in the data. For each significant test, a general two-sided significance level of 5% was applied. All statistical analyses were performed with SAS software (SAS Institute, Cary, NC) version 8.1.

RESULTS

Thin wall assumption. Average measured OD and ID at each pressure and for each condition are provided in Table 1. To validate the thin wall assumption, the ratio of inner radius to WT was calculated for each vessel and then averaged across groups. The thin wall assumption was found to be valid for all vessels, for all pressures >5 mmHg. At 5 mmHg, some vessels could not be considered "thin;" however, no mechanical properties were measured at this pressure. The average ratios of inner radius to WT for 0-day, 10-day, and 15-day vessels were 10.6 (SD 2.3), 11.8 (SD 2.2), and 12.9 (SD 2.6), respectively, at 5 mmHg. As the pressure increased, the average ratios increased such that, between 10 and 20 mmHg, where elastic modulus was measured, the thin wall assumption held for all vessels. The ratios for 0-day, 10-day, and 15-day vessels were 36.2 (SD 9.2), 26.8 (SD 5.1), and 28.1 (SD 4.6), respectively, at 25 mmHg.

Static behavior. Optically measured main PA OD increased significantly with hypoxia and imposed transmural pressure (Table 1). At the baseline pressure of 5 mmHg, the 10- and

Table 1. *Optically measured PA dimensions*

Transmural Pressure	Groups		
	0 Day	10 Day	15 Day
5 mmHg			
OD	546±22	558±38	592±24*†
ID	500±23	507±39	540±29*†
L	2.2±0.2	2.4±0.1	2.5±0.1
10 mmHg			
OD	610±24	619±26	653±16*†
ID	570±27	581±27	608±16*†
15 mmHg			
OD	698±37	676±35	712±19†
ID	661±43	639±39	670±22
20 mmHg			
OD	811±59	733±56*	773±29
ID	781±61	700±61*	737±32
25 mmHg			
OD	960±60	806±61*	847±42*
ID	932±67	778±64*	813±41*
10 mmHg			
OD	606±24	609±37	638±35
ID	568±27	569±38	596±38

Data are means ± SD. Optically measured pulmonary artery (PA) outer (OD) and inner diameters (ID; in μm) for the 0-, 10-, and 15-day groups taken at baseline transmural pressure of 5 mmHg and 15 s after each static pressure step. Axial length (*L*; in mm) is provided at 5 mmHg. Final step to 10 mmHg (*bottom* 2 rows) was performed to verify the absence of plastic deformation from the mechanical testing protocol. Statistical significance of differences was assessed between experimental groups by ANOVA. *$P < 0.05$ vs. 0-day group; †$P < 0.05$ vs. 10-day group.

15-day hypoxic vessel ODs were 2 and 8% larger than the control, 0-day vessel ODs, respectively. At the highest transmural pressure of 25 mmHg, the 10- and 15-day hypoxic vessels were 16 and 12% smaller than the 0-day vessels, respectively. The ODs measured during a final step to 10 mmHg (the second to last row in Table 1) were <2% different on average from the ODs measured during the first step to 10 mmHg, indicating the absence of plastic deformation.

The static stretch response of the vessels to steps in pressure measured isochronally was greater in control vessels than in hypoxic vessels at all pressures tested (Fig. 2; note that λ is dimensionless). That is, control vessels always stretched more circumferentially in response to transmural pressure increases than hypoxic vessels. Differences were not significant for the 10-mmHg step but were increasingly significant as the pressure steps increased in magnitude, with the greatest difference at 25 mmHg ($P < 0.0001$). There were no significant differences between the stretch responses of the two hypoxic groups.

Dynamic behavior. Effective dynamic circumferential elastic moduli for the 0-, 10-, and 15-day vessels were 222 (SD 35), 280 (SD 53), and 296 kPa (SD 50), respectively (Fig. 3). Although the two hypoxic groups were not significantly different from each other, both were significantly different from the control group ($P < 0.02$). Damping coefficients for the 0-, 10-, and 15-day vessels were 0.033 (SD 0.016), 0.063 (SD 0.017), and 0.054 (SD 0.014), respectively (Fig. 4; note that damping coefficient is dimensionless). Again, the two hypoxic groups were not significantly different from each other, but both were significantly different from the control group ($P < 0.002$).

WT, SMC, and protein content. Complete histological measurements were performed on seven 0-day, eight 10-day hypoxic, and eight 15-day hypoxic tissue specimens. Two tissue blocks cracked upon thawing from −80 to −20°C and could not be sectioned (one 0-day and one 10-day); one tissue block ran out before sections for all the staining protocols were obtained (15-day). Histologically measured WT values increased significantly with hypoxia exposure from 21 μm (SD 4) at 0 days to 29 (SD 5) and 33 μm (SD 4) at 10 and 15 days, respectively ($P < 0.002$ and $P < 0.0001$, respectively, vs. control). IDs and ODs could not be reliably measured because many sections were undulating segments of circles rather than complete circles or ellipses, since these specimens were not fixed at pressure. In addition, these histologically measured WTs may overestimate in vivo WTs for the same reason. However, we have assumed that the degree of overestimation remains constant with respect to hypoxia exposure.

Representative images of control and 10-day hypoxic vessels stained for VVG and SR are shown in Fig. 5. The average percentages of elastin in the artery wall of the 0-, 10-, and

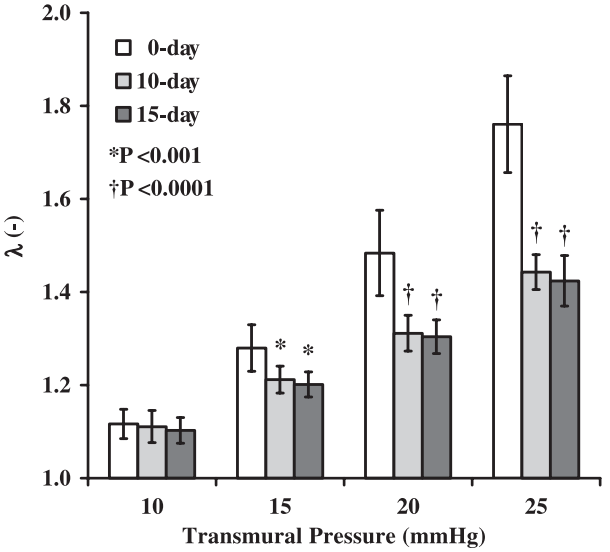

Fig. 2. Circumferential isochronal stretch ratio λ (*Eq. 2*) for each pressure step (15 s after step) for the 0-, 10-, and 15-day groups. Bars represent means ± SD. *P and †P values compared with control.

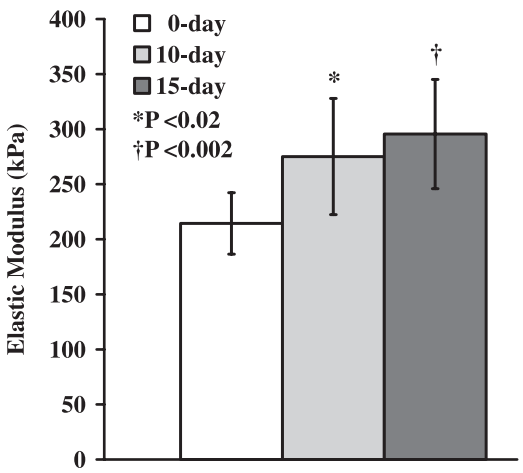

Fig. 3. Effective circumferential elastic modulus E at the midstrain point for the 0-, 10-, and 15-day groups. Bars represent means ± SD. *P and †P values compared with control.

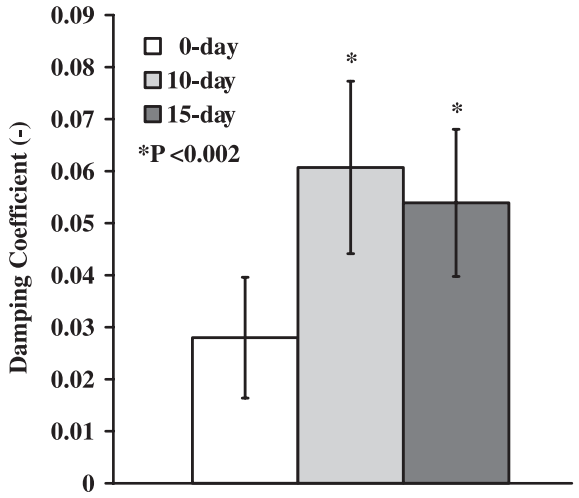

Fig. 4. Damping coefficient for the 0-, 10-, and 15-day groups. Bars represent means ± SD. *P value compared with control.

15-day groups were 29 (SD 3), 30 (SD 5), and 29% (SD 4), respectively. The average percentages of collagen for the three groups were 46 (SD 5), 52 (SD 4), and 52% (SD 2), respectively, and the average computed percentages of SMCs were 24 (SD 6), 18 (SD 7), and 19% (SD 4), respectively. Whereas the percent elastin in the arterial wall did not change significantly with hypoxia exposure, the percent collagen ($P < 0.02$ for both 10-day vs. control and 15-day vs. control) and percent SMCs did ($P < 0.05$ for 10-day vs. control).

In addition, collagen, elastin, and SMC thickness (percent protein multiplied by WT for a given vessel) were analyzed for changes with hypoxia exposure. In particular, elastin thickness increased after 10 and 15 days ($P < 0.02$ and $P < 0.002$ vs. control, respectively), and collagen thickness increased after 10 and 15 days ($P < 0.0001$ vs. control for both). Collagen thickness also increased between 10 and 15 days ($P < 0.02$). SMC thickness did not change significantly (Fig. 6, *A–C*).

Qualitatively, it was observed that most of the collagen accumulation was adventitial, whereas the elastin accumulation was in the intima and media.

Mechanobiological correlations. To assess the presumptive correlative relationships between mechanical-functional and biological-structural indicators of remodeling, effective circumferential dynamic modulus was plotted vs. collagen thickness and vs. the sum of elastin and collagen thicknesses (Fig. 7, *A* and *B*). Damping coefficient was plotted vs. SMC thickness (Fig. 7*C*). To assess the linearity of these relationships, the regression analysis coefficient of determination (R^2) was measured; to assess the trends in these relationships, the Spearman's rank correlation coefficient (r_s) was measured. For the latter, a P value is reported if significant ($P < 0.05$).

Between effective dynamic circumferential elastic modulus and collagen thickness, there was a moderate linearity ($R^2 = 0.37$), with a significant trend toward higher moduli with higher collagen thickness ($r_s = 0.55$, $P < 0.005$). Between modulus and the sum of elastin and collagen thickness, there was a moderate linearity ($R^2 = 0.44$), with a significant trend toward higher moduli with higher elastin and collagen thick-

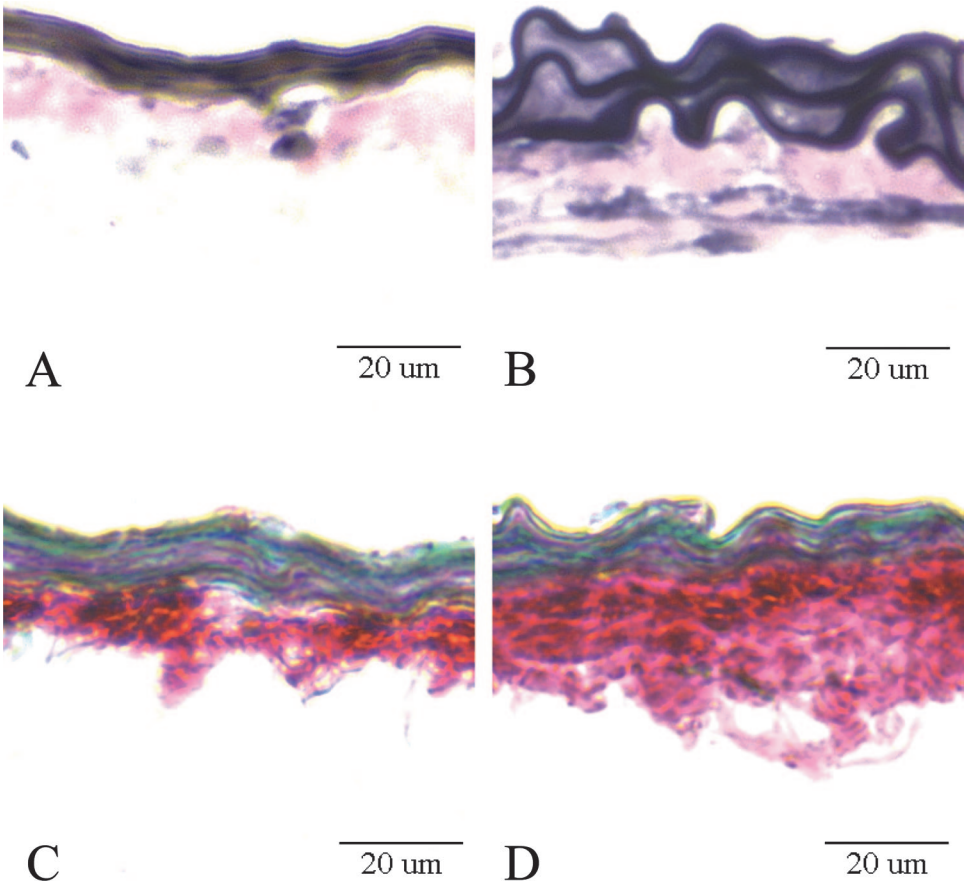

Fig. 5. Representative Verhoff Van Geisen (VVG; *A* and *B*) and picro-sirius red (SR; *C* and *D*) staining of 0-day (*A* and *C*) and 10-day hypoxic (*B* and *D*) vessels. For VVG, elastin stains black and cell nuclei appear dark. For SR, collagen appears red. Scale bar is 20 μm for all images.

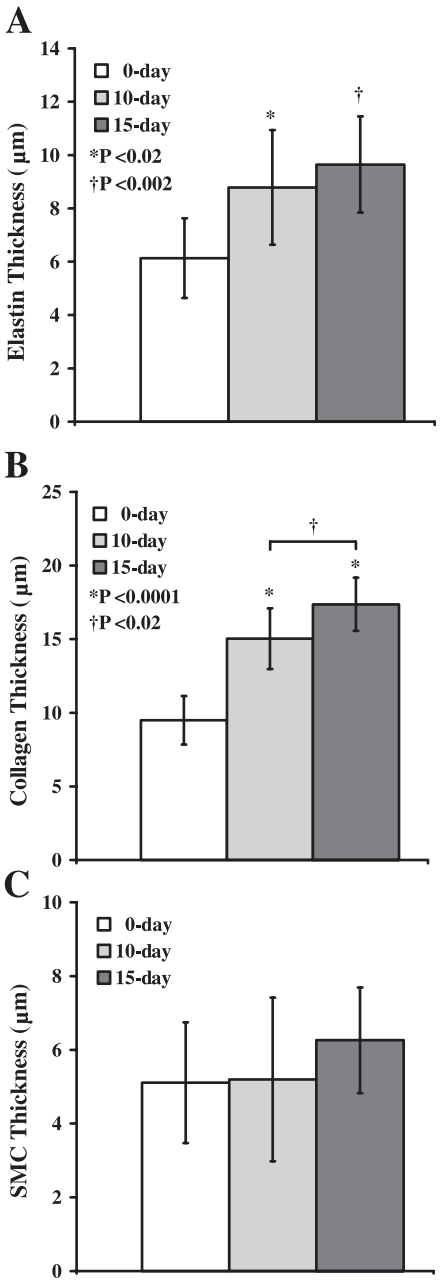

Fig. 6. Calculated equivalent elastin (*A*), collagen (*B*), and smooth muscle cell (SMC; *C*) thickness for the 0-day, 10-day, and 15-day groups. Bars represent means ± SD. *P and †P values compared with control.

ness (r_s = 0.70, $P < 0.0002$). Finally, between damping coefficient and SMC thickness, there was essentially no linearity (R^2 = 0.00) and no significant trend.

Note, these correlations between mechanical-functional behavior in the left PA and biological-structural features in the right PA assume certain similarities between the right and left PAs. We did not randomize mechanical and biological assays to the right and left sides because the right PA was consistently shorter and larger (in diameter) than the left, which would have introduced more variability into the mechanical results. Preliminary studies suggested that the right and left PA WT and extracellular matrix protein content at 0, 10, and 15 days were similar to that of the left PAs. The larger diameter of the right PA would alter the measured mechanical properties, but the effect on the correlation should only be a change in slope of the modulus-extracellular matrix thickness curve, not in the goodness of fit; there should be no effect of the length difference, since axial effects were not considered.

Also note that these correlative relationships do not depend on absolute values of collagen, elastin, or SMC thickness but instead on the changes in those thicknesses with hypoxia. Thus

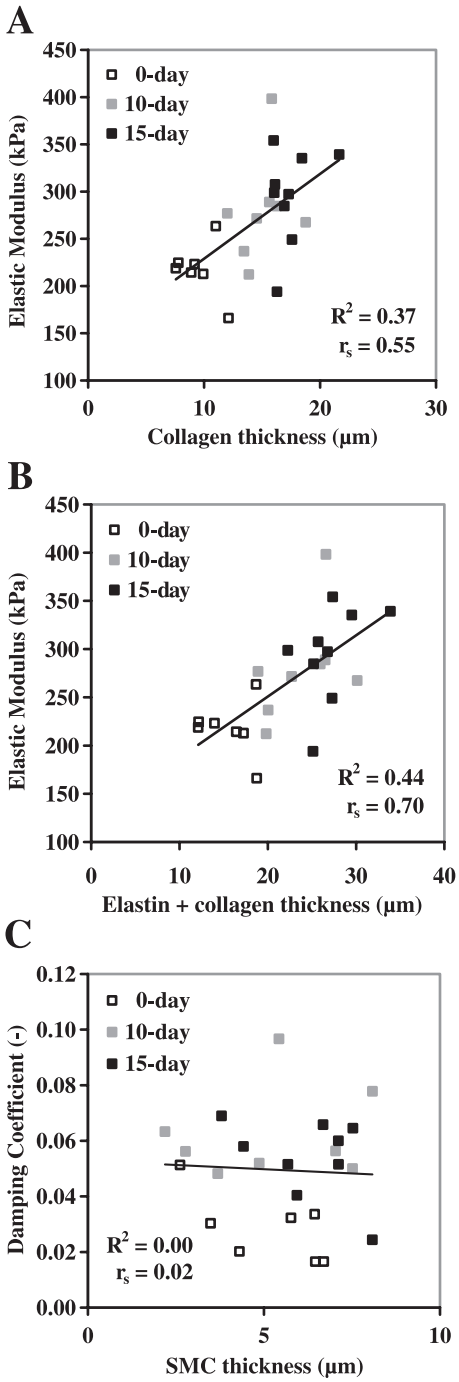

Fig. 7. Correlations between effective elastic modulus and collagen thickness ($P < 0.005$; *A*), effective elastic modulus and sum of elastin and collagen thickness ($P < 0.0002$; *B*), and damping coefficient and SMC thickness (*C*) for all vessels for which histological data were available. R^2 and r_s values are provided (see *Statistics* for details).

possible errors in the histologically measured WT values due to the lack of pressure fixation should not affect the coefficients of correlation or their significance.

DISCUSSION

Our results show that after 10 and 15 days of hypoxia, the main PAs of mice stretch less in response to pressure increases, have higher circumferential elastic moduli, and have higher damping coefficients. The results also show increased wall thickness with a decrease in SMC percentage, no change in elastin, and an increase in collagen in response to increasing durations of hypoxia-induced hypertension. The measured changes in circumferential stiffness in the left PA correlated with collagen thickness and the sum of collagen and elastin thickness in the right PA; however, the measured changes in damping coefficient in the left PA did not correlate with SMC thickness in the right PA. These results are discussed in more detail in the following sections.

Static behavior. Our static stretch-pressure data demonstrated significant differences between control and hypoxic vessels. Previously, static pressure-diameter and pressure-stretch relationships for PAs have been studied in intact lungs using radio-opaque perfusion and X-ray visualization techniques (2, 28, 42). In the largest PAs of the cat (1,000–1,600 μm), stretch was shown to increase linearly with pressure between 0 and 15 mmHg, with a slope of ~3.5%/mmHg (42). By way of comparison, the slope of the stretch-pressure curve for control vessels in our study was ~3.75%/mmHg (i.e., stretch increased from 100 to 175% as pressure increased from 5 to 25 mmHg), while the 10- and 15-day vessels had slopes of 2.22 and 2.12%/mmHg, respectively. Although these simple slope parameters show that the hypoxic vessels act stiffer than the control vessels as predicted, it should be noted that all tissue is mechanically nonlinear. The tissue is acting linearly in this relatively small pressure range, but under larger stresses, all vessels show decreasing rate of stretch with increasing pressure.

Dynamic behavior. As measured dynamically, the effective circumferential elastic moduli of mouse left main PAs increased significantly with hypoxia. These results correlate with the findings in humans that patients with primary pulmonary hypertension have increased stiffness in their pulmonary vasculature (24). In a short-term study on rats exposed to hypoxia, the circumferential elastic moduli of PAs increased from 171 ± 13 kPa after 0 h to 178 ± 34 kPa after 12 h and 187 ± 14 kPa after 24 h (19). However, these calculations were based on quasi-static pressure-diameter measurements; that is, pressure was incremented stepwise by 15-mmHg increments (from 30 to 70 mmHg) instead of continuously.

Without in-depth knowledge of tissue viscoelastic properties, the effects of quasi-static testing on elastic modulus cannot be estimated, but certainly dynamic testing will yield data that better predict the in vivo behavior of PAs. Indeed, Cox (6) found frequency-dependent differences in elastic modulus in canine PAs between 0.002 and 0.1 Hz but not between 0.1 and 10 Hz. For this study, the testing frequency was in the middle of the frequency-dependent range: 0.014 Hz. Thus, although these low-frequency dynamic measurements are a better estimate of in vivo behavior than static measurements, higher-frequency measurements are required to predict behavior up to 10 Hz, which is a normal heart rate for the mouse.

The PA damping coefficient calculated from the dynamic stress-strain curve nearly doubled from the 0-day, control condition to the 10- and 15-day conditions. Cox (6) also observed damping behavior in canine PAs; qualitatively, damping decreased with SMC activation. In these studies, the effects of SMC activity on damping were not tested. Functionally, higher damping values in the hypoxic vessels indicate more energy dissipation through inelastic mechanisms during systolic pressure loading. Thus with increased damping, the work required of the right heart increases, adding to the long-term stress on the heart and risk of ischemia. Both damping and stiffness changes may adversely affect ventricular-vascular coupling.

Wall thickness, SMC, and protein content. As predicted, wall thickness measured histologically increased with pulmonary hypertension, primarily by collagen and elastin accumulation. Wall thickness increased 38% after 10 days of hypertension. Over the course of 24 h in rat PAs, Huang et al. (19) observed a statistically insignificant increase from 65.8 to 66.1 μm. The increase in wall thickness in our study was due to increases in both collagen and elastin thickness, with no change in SMC thickness. In fact, the percent SMCs in the vessel wall tended to decrease, whereas the percent elastin was constant and the percent collagen increased. Note, phenotypic changes in SMCs, from a contractile to a proliferative phenotype, were not measured, nor were other potentially important vascular wall elements such as fibronectin, proteoglycans, and degree of protein cross-linking. The increases in collagen and elastin thickness were most likely due to the upregulation of procollagen and tropoelastin genes in response to hypoxia-induced pulmonary hypertension as previously described for calves (8, 38).

Mechanobiological correlations. The real advantage of performing both mechanical-functional and biological-structural measurements on contralateral arteries during remodeling is the ability to correlate the mechanical changes with the biological changes. As demonstrated by Fig. 7, our hypothesis that hypoxia would increase elastic modulus by collagen accumulation was upheld. However, SMC thickness did not correlate with the damping coefficient, disproving our hypothesis that the thickness of the SMC layer controls dynamic vascular tissue damping. As noted above, the effects of SMC activity on damping were not tested. In addition, phenotypic changes in SMCs were not tested and may have affected the viscous behavior of the arteries even in the absence of SMC activity. Indeed, because SMC phenotype, viability, and vasoreactivity were not assessed, there is no evidence that the SMCs contributed functionally to the mechanical properties of the tissue except in a passive way. Other vascular wall elements such as proteoglycans and ground substances not measured in this study may have contributed to increased damping (26). As tissue viscoelastic properties such as damping become better understood by measurements such as these, their relationship to vascular biology and structure may become clearer.

The correlations found here between effective elastic modulus and collagen thickness, as well as between modulus and the sum of elastin and collagen thickness, were performed for all conditions to look for overall changes in the mechanobiological behavior of PAs in response to pulmonary hypertension. Subgroup correlations (for 0-, 10-, and 15-day subgroups)

were also analyzed, but none were significant. It is interesting to note that some of the correlative relationships for individual groups appear different from the relationships for all groups. We would speculate that these trends indicate the presence of one or more vascular wall elements (such as degree of protein cross-linking, SMC phenotype, viability, and vasoreactivity) not measured in this study.

Experimental considerations. In these experiments, we did not measure the zero-stress state of the arteries or use the zero-stress state as the reference state in the strain calculations. Instead, the state at 5 mmHg was used as the reference state in the stress, strain, and elastic modulus calculations. In rats exposed to 10 days of hypoxia, residual stress measurements on main PAs have shown that the outer wall grew more circumferentially than the inner wall, which had the effect of equalizing the distribution of stress in the radial direction at the loaded state (15). The PAs in this study were thin enough that the radial distribution of stress could be ignored, but future studies to confirm radial differences in growth rates in mouse PAs could yield further insight into the biomechanics of pulmonary vascular remodeling.

As noted above, the vessels were not fixed at pressure, so the histological wall thickness measurements likely overestimate the in vivo values. We have assumed that the degree of overestimation remains constant with respect to hypoxia; however, this assumption may not be valid. Indeed, the degree of difference between pressurized wall thickness and unpressurized wall thickness may be affected by hypoxia-induced pulmonary vascular remodeling. This is a confounding variable that may have artifactually affected the differences between control and hypoxic wall, collagen, elastin, and SMC thickness values. In that case, the percent changes in collagen, elastin, and SMC are a better measure of the biological aspects of remodeling.

We cannot exclude the possibility of axial remodeling with 10 and 15 days of exposure to hypoxia. In the absence of reliable in vivo PA lengths for mice, we prestretched all vessels to 112% of their rest length. According to the data of Huang et al. (19) for rat PAs, in vivo axial length ranges from 140 to 160% of the rest length under normal conditions, and 1 day of hypoxia leads to no significant change in the axial stretch ratio; however, in our hands this degree of axial stretch led to cannula pull-off, catastrophically ending the experiment.

To perform the mechanical property calculations, we assumed the vessel walls were thin, incompressible, and homogeneous. The thin wall assumption was validated here, and the incompressibility of isolated mouse PAs has been shown elsewhere (11). Vasculature is inherently heterogeneous in the radial direction due to the layered nature of arteries and veins and often heterogeneous in the axial direction. However, the assumption of radial homogeneity is appropriate to a thin wall analysis. Insofar as we measured axial changes in biological properties, no differences were detected.

Finally, tissue injury or damage also may have affected our results. As shown by Von Maltzahn et al. (41) in bovine carotid arteries, loss of adventitia will reduce the measured elastic modulus in isolated arteries. Extreme care was taken during excision to limit damage due to handling. However, contraction/relaxation studies were not performed to ensure that endothelial and SMCs were intact and viable. Nevertheless, identical techniques were used to harvest right and left PAs; the absence of either intimal or adventitial damage evident histologically in right PAs strongly suggests that the mechanically tested left PAs were similarly undamaged.

In conclusion, this study has demonstrated changes in mechanical-functional properties in the mouse main PAs with hypoxia-induced hypertension and changes in the biological-structural properties and quantitative structure-function relationships. In particular, in response to hypoxia-induced hypertension, the main PAs of mice had decreased stretch-response statically, increased effective stiffness dynamically, and increased damping dynamically. The measured changes in circumferential effective stiffness correlated with collagen thickness as well as the sum of collagen and elastin thickness in contralateral arteries. Only with simultaneous performance of mechanical and biological assays in contralateral vessels could these relationships have been quantified. Uncovering the correlative relationships between mechanical stimuli (such as high blood pressure) and biological responses (such as collagen and elastin accumulation), and between these biological responses and mechanical property changes (such as increased effective stiffness), is critical to understanding the progression of vascular remodeling in pulmonary hypertension and possibly to designing new treatments to prevent it.

ACKNOWLEDGMENTS

We thank Roderic Lakes for helpful discussions.

GRANTS

Funding support from National Institutes of Health COBRE grant P20RR15557, the University of Wisconsin-Madison College of Engineering, the Wisconsin Alumni Research Foundation, and the Whitaker Foundation (Grant RG-02-0618) is gratefully acknowledged.

REFERENCES

1. **Bancroft J and Stevens A.** *Theory and Practice of Histological Techniques*. New York: Churchilll Livingstone, 1982.
2. **Caro CG and Saffman PG.** Extensibility of blood vessels in isolated rabbit lungs. *J Physiol* 178: 193–210, 1965.
3. **Chesler NC, Figueroa-Thompson J, and Millburne K.** Measurements of mouse pulmonary artery biomechanics. *J Biomech Eng* 126: 309–314, 2004.
4. **Chesler NC, Ku DN, and Galis ZS.** Transmural pressure induces matrix-degrading activity in porcine arteries ex vivo. *Am J Physiol Heart Circ Physiol* 277: H2002–H2009, 1999.
5. **Cotran RS, Kuman V, Collins T, Robbins SL, and Schmitt B.** *Robbins Pathologic Basis of Disease*. Philadelphia, PA: WB Saunders, 1999.
6. **Cox RH.** Viscoelastic properties of canine pulmonary arteries. *Am J Physiol Heart Circ Physiol* 246: H90–H96, 1984.
7. **DiCarlo VS, Chen SJ, Meng QC, Durand J, Yano M, Chen YF, and Oparil S.** ETA-receptor antagonist prevents and reverses chronic hypoxia-induced pulmonary hypertension in rat. *Am J Physiol Lung Cell Mol Physiol* 269: L690–L697, 1995.
8. **Durmowicz AG, Parks WC, Hyde DM, Mecham RP, and Stenmark KR.** Persistence, re-expression, and induction of pulmonary arterial fibronectin, tropoelastin, and type I procollagen mRNA expression in neonatal hypoxic pulmonary hypertension. *Am J Pathol* 145: 1411–1420, 1994.
9. **Elton TS, Oparil S, Taylor GR, Hicks PH, Yang RH, Jin H, and Chen YF.** Normobaric hypoxia stimulates endothelin-1 gene expression in the rat. *Am J Physiol Regul Integr Comp Physiol* 263: R1260–R1264, 1992.
10. **Fagan KA, Fouty BW, Tyler RC, Morris KG Jr, Hepler LK, Sato K, LeCras TD, Abman SH, Weinberger HD, Huang PL, McMurtry IF, and Rodman DM.** The pulmonary circulation of homozygous or heterozygous eNOS-null mice is hyperresponsive to mild hypoxia. *J Clin Invest* 103: 291–299, 1999.
11. **Faury G, Maher GM, Li DY, Keating MT, Mecham RP, and Boyle WA.** Relation between outer and luminal diameter in cannulated arteries. *Am J Physiol Heart Circ Physiol* 277: H1745–H1753, 1999.

12. **Fike CD, Pfister SL, Kaplowitz MR, and Madden JA.** Cyclooxygenase contracting factors and altered pulmonary vascular responses in chronically hypoxic newborn pigs. *J Appl Physiol* 92: 67–74, 2002.
13. **Fung YC.** *Biomechanics: Motion, Flow, Stress and Growth*. New York: Springer-Verlag, 1990.
14. **Fung YC.** *Biomechanics: Mechanical Properties of Living Tissues*. New York: Springer-Verlag, 1993.
15. **Fung YC and Liu SQ.** Changes of zero-stress state of rat pulmonary arteries in hypoxic hypertension. *J Appl Physiol* 70: 2455–2470, 1991.
16. **Gascon-Barre M, Huet PM, Belgiorno J, Plourde V, and Coulombe PA.** Estimation of collagen content of liver specimens. Variation among animals and among hepatic lobes in cirrhotic rats. *J Histochem Cytochem* 37: 377–381, 1989.
17. **Hayashi K, Stergiopulos N, Meister JJ, Greenwald SE, and Rachev A.**Techniques in the determination of the mechanical properties and constitutive laws of arterial walls. In: *Cardiovascular Techniques*, edited by Leonedes C. Boca Raton, FL: CRC, 2001, p. 6-1–6-61.
18. **Hislop A and Reid L.** New findings in pulmonary arteries of rats with hypoxia-induced pulmonary hypertension. *Br J Exp Pathol* 57: 542–554, 1976.
19. **Huang W, Delgado-West D, Wu JT, and Fung YC.** Tissue remodeling of rat pulmonary artery in hypoxic breathing. II. Course of change of mechanical properties. *Ann Biomed Eng* 29: 552–562, 2001.
20. **Humphrey JD.** *Cardiovascular Solid Mechanics: Cells, Tissues and Organs*. New York: Springer, 2002.
21. **Jeffery TK and Wanstall JC.** Pulmonary vascular remodeling: a target for therapeutic intervention in pulmonary hypertension. *Pharmacol Ther* 92: 1–20, 2001.
22. **Katayose D, Ohe M, Yamauchi K, Ogata M, Shirato K, Fujita H, Shibahara S, and Takishima T.** Increased expression of PDGF A- and B-chain genes in rat lungs with hypoxic pulmonary hypertension. *Am J Physiol Lung Cell Mol Physiol* 264: L100–L106, 1993.
23. **Lakes R.** *Viscoelastic Solids.* Boca Raton, FL: CRC, 1998.
24. **Laskey WK, Ferrari VA, Palevsky HI, and Kussmaul WG.** Pulmonary artery hemodynamics in primary pulmonary hypertension. *J Am Coll Cardiol* 21: 406–412, 1993.
25. **Li H, Chen SJ, Chen YF, Meng QC, Durand J, Oparil S, and Elton TS.** Enhanced endothelin-1 and endothelin receptor gene expression in chronic hypoxia. *J Appl Physiol* 77: 1451–1459, 1994.
26. **Ling SC and Chow CH.** The mechanics of corrugated collagen fibrils in arteries. *J Biomech* 10: 71–77, 1977.
27. **Liu SQ.** Alterations in structure of elastic laminae of rat pulmonary arteries in hypoxic hypertension. *J Appl Physiol* 81: 2147–2155, 1996.
28. **Maloney JE, Rooholamini SA, and Wexler L.** Pressure-diameter relations of small blood vessels in isolated dog lung. *Microvasc Res* 2: 1–12, 1970.
29. **Marshall BE and Marshall C.** Pulmonary hypertension. In: *The Lung: Scientific Foundations* (2nd ed.), edited by Crystal RG. Philadelphia, PA: Lippincot-Raven, 1997, p. 1581–1588.
30. **Meyrick B and Reid L.** The effect of continued hypoxia on rat pulmonary arterial circulation. An ultrastructural study. *Lab Invest* 38: 188–200, 1978.
31. **Milnor WR, Conti CR, Lewis KB, and O'Rourke MF.** Pulmonary arterial pulse wave velocity and impedance in man. *Circ Res* 25: 637–649, 1969.
32. **Ozaki M, Kawashima S, Yamashita T, Ohashi Y, Rikitake Y, Inoue N, Hirata KI, Hayashi Y, Itoh H, and Yokoyama M.** Reduced hypoxic pulmonary vascular remodeling by nitric oxide from the endothelium. *Hypertension* 37: 322–327, 2001.
33. **Paulus MJ, Gleason SS, Kennel SJ, Hunsicker PR, and Johnson DK.** High resolution X-ray computed tomography: an emerging tool for small animal cancer research. *Neoplasia* 2: 62–70, 2000.
34. **Perkett EA, Lyons RM, Moses HL, Brigham KL, and Meyrick B.** Transforming growth factor-β activity in sheep lung lymph during the development of pulmonary hypertension. *J Clin Invest* 86: 1459–1464, 1990.
35. **Quinlan TR, Li D, Laubach VE, Shesely EG, Zhou N, and Johns RA.** eNOS-deficient mice show reduced pulmonary vascular proliferation and remodeling to chronic hypoxia. *Am J Physiol Lung Cell Mol Physiol* 279: L641–L650, 2000.
36. **Rabinovitch M, Gamble W, Nadas AS, Miettinen OS, and Reid L.** Rat pulmonary circulation after chronic hypoxia: hemodynamic and structural features. *Am J Physiol Heart Circ Physiol* 236: H818–H827, 1979.
37. **Rubin LJ.** Primary pulmonary hypertension. *N Engl J Med* 336: 111–117, 1997.
38. **Stenmark KR, Durmowicz AG, Roby JD, Mecham RP, and Parks WC.** Persistence of the fetal pattern of tropoelastin gene expression in severe neonatal bovine pulmonary hypertension. *J Clin Invest* 93: 1234–1242, 1994.
39. **Stenmark KR, Gerasimovskaya E, Nemenoff RA, and Das M.** Hypoxic activation of adventitial fibroblasts: role in vascular remodeling. *Chest* 122: 326S–334S, 2002.
40. **Voelkel NF and Tuder RM.** Hypoxia-induced pulmonary vascular remodeling: a model for what human disease? *J Clin Invest* 106: 733–738, 2000.
41. **Von Maltzahn WW, Warriyar RG, and Keitzer WF.** Experimental measurements of elastic properties of media and adventitia of bovine carotid arteries. *J Biomech* 17: 839–847, 1984.
42. **Yen RT, Fung YC, and Bingham N.** Elasticity of small pulmonary arteries in the cat. *J Biomech Eng* 102: 170–177, 1980.
43. **Zuckerman BD, Orton EC, Latham LP, Barbiere CC, Stenmark KR, and Reeves JT.** Pulmonary vascular impedance and wave reflections in the hypoxic calf. *J Appl Physiol* 72: 2118–2127, 1992.